A Theoretical Study of the Primary Oxo Transfer Reaction of a Dioxo Molybdenum(VI) Compound with Imine Thiolate Chelating Ligands: A Molybdenum Oxotransferase Analogue

Lisa M. Thomson and Michael B. Hall*

Contribution from the Department of Chemistry, Texas A&M University, College Station, Texas 77842

Received September 5, 2000. Revised Manuscript Received February 19, 2001

Abstract: The reaction mechanism of an analogue system of the molybdenum oxotransferases was investigated at the density functional (B3P86) level of theory. Kinetic measurements by Schultz and Holm suggest that the reaction MoO_2(*t*-BuL-NS)$_2$ + X → MoO(*t*-BuL-NS)$_2$ + OX (*t*-BuL-NS = bis(4-*tert*-butylphenyl)-2-pyridylmethanethiolate(1−)) occurs through an associative transition state. Our results on the model reaction, $MoO_2(SCH_2CHNH)_2 + P(CH_3)_3 \rightarrow MoO(SCH_2CHNH)_2 + OP(CH_3)_3$, support this hypothesis, and indicate that this reaction proceeds through a two-step mechanism via an associative intermediate. The $\Delta H^{\ddagger}$ for the first, and rate-determining, step was predicted to be 9.4 kcal/mol, and $\Delta H^{\ddagger}$ for the second step (release of the $OP(CH_3)_3$ product) was predicted to be 3.3 kcal/mol. These results are in good agreement with the experimental system, for which the rate determining $\Delta H^{\ddagger} = 9.6(6)$ kcal/mol. Shultz and Holm's experimental model undergoes a significant ligand rearrangement in the oxo transfer reaction: the reactant, MoO_2(*t*-BuL-NS)$_2$, has a *trans*-S arrangement of the ligands, while the product, MoO(*t*-BuL-NS)$_2$, has a *trans*-N arrangement. To investigate the driving force behind the ligand rearrangement, four model compounds, that systematically removed the unsaturation at the N and the chelate character of the ligands, were modeled at the B3P86 level of theory. For all models of the dioxo species, the *trans*-N isomer was higher in energy than the *trans*-S isomer. The analysis of these results indicated that a trans influence accounts for approximately 16% of the energy difference, the unsaturation at the nitrogens accounts for ≈26%, and the ring strain from the chelator accounts for ≈58% of the energy difference between the two isomers (*trans*-N and *trans*-S). For all models of the monooxo species, only the *trans*-N species was a stable geometry. Therefore, for the reverse oxo transfer reaction, ligand rearrangement must occur after or during the attack of the OX substrate.

Introduction

Molybdenum-containing enzymes are a broad class of enzymes that are essential for the metabolism of carbon, nitrogen, and sulfur in a wide variety of organisms.[1] All of the well-characterized molybdoenzymes have been found to have one or two metal-binding pterin-substituted 1,2-enedithiolate ligands (MPT) bound to the molybdenum in the active site.[2−5] Along with the MPT ligands there may be zero, one, or two terminal oxo groups, and/or a terminal sulfur group.[2−5] On the basis of the differences in the coordination at the active site, the molybdenum-containing enzymes have been classified into the families[1b] shown in Scheme 1. Even though the names of the different enzymes are based on their reaction with a specific substrate, it has been found that some can catalyze more than one substrate (i.e. they are not necessarily selective) in vivo and in vitro.[6] Some of the more common molyboenzymes are DMSO reductase,[1,2] sulfite oxidase,[1,7] xanthine oxidase,[1,4,8] and nitrate reductase.[1]

Many of the enzymes are molybdenum oxotransferases that catalyze the overall reaction shown in eq 1, where X is the

$$X + H_2O \rightleftharpoons OX + 2H^+ + 2e^- \qquad (1)$$

oxygen accepting substrate. The molybdenum oxotransferases that do not contain a sulfido group are thought to proceed through a primary oxo transfer reaction[1c] as shown in eq 2. Studying the structures of the active site in the molybdenum

(1) (a) Pilato, R. S.; Stiefel, E. I. *Bioinorganic Catalysis*, 2nd ed.; Reedijk, J., Bouwman, E., Eds.; Marcel Dekker: New York, 1999; Chapter 6, pp 88−152. (b) Hille, R. *Chem. Rev.* **1996**, *96*, 2757. (c) Holm, R. H. *Coord. Chem. Rev.* **1990**, *100*, 183. (d) Bray, R. C. *Q. Rev. Biophys.* **1988**, *21*, 299.

(2) (a) McAlpine, A. S.; McEwan, A. G.; Bailey, S. *J. Mol. Biol.* **1998**, *275*, 613. (b) Schneider, F.; Lowe, J.; Huber, R.; Schindelin, H.; Kisker, C.; Knablein, J. *J. Mol. Biol.* **1996**, *263*, 53. (c) McAlpine, A. S.; McEwan, A. G.; Shaw, A. L.; Bailey, S. *J. Biol. Inorg. Chem.* **1997**, *2*, 690. (d) Schindelin, H.; Kisker, C.; Hilton, J.; Rajagopalan, K. V.; Rees, D. C. *Science* **1996**, *272*, 1615.

(3) Kisker, C.; Schindelin, H.; Pacheco, A.; Wehbi, W. A.; Garrett, R. M.; Rajagopalan, K. V.; Enemark, J. H.; Rees, D. C. *Cell* **1997**, *91*, 973.

(4) (a) Romao, M. J.; Archer, M.; Moura, I.; Moura, J. J. G.; Legall, J.; Engh, R.; Schneider, M.; Hof, P.; Huber, R. *Science* **1995**, *270*, 1170. (b) Czjzek, M.; Dos Santos, J. P.; Pommier, J.; Giordano, G.; Mejean, V.; Haser, R. *J. Mol. Biol.* **1998**, *284*, 435.

(5) Huber, R.; Hof, P.; Duarte, R. O.; Moura, J. J. G.; Moura, I.; Liu, M.-Y.; LeGall, J.; Hill, R.; Archer, M.; Romao, M. J. *Proc. Natl. Acad. Sci. U.S.A.* **1996**, *93*, 8856.

(6) (a) Adams, M. W. W.; Mortenson, L. E. *Metal Ions in Biology, Molydbenum Enzymes*; Spiro, T. G., Ed.; Wiley & Son: New York, 1985;, pp. 519−594. (b) Clarke, G. J.; Ward, F. B. *J. Gen. Microbiol.* **1988**, *134*, 379. (c) Kirstein, K.; Bock, E. *Arch. Microbiol.* **1993**, *160*, 447. (d) Krueger, B.; Meyer, O.; Nagel, M.; Andreesen, J. R.; Meineke, M.; Bock, E.; Bluemle, S.; Zumft, W. G. *FEMS Microbiol. Lett.* **1987**, *48*, 225. (e) Miencke, M.; Bock, E.; Kastrau, D.; Kroneck, P. M. H. *Arch. Microbiol.* **1992**, *158*, 127. (f) Sundermeyer-Klinger, H.; Meyer, W.; Warninghoff, B.; Bock, E. *Arch. Microbiol.* **1984**, *140*, 153. (g) Lin, J. T.; Stewart, V. *Adv. Microb. Physiol.* **1998**, 1.

(7) Xiao, Z.; Young, C. G.; Enemark, J. H.; Wedd, A. G. *J. Am. Chem. Soc.* **1992**, *114*, 9194.

(8) Hille, R.; Sprecher, H. *J. Biol. Chem.* **1987**, *262*, 10914.

10.1021/ja003258y CCC: $20.00
Published on Web 04/10/2001

Scheme 1

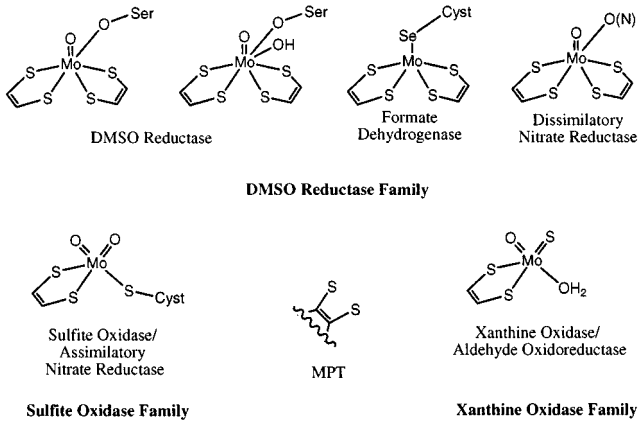

$$Mo^{VI}O_2L_2 + X \rightleftharpoons Mo^{IV}OL_2 + OX \qquad (2)$$

oxotranferase enzymes is difficult due to the complexity and delicate nature of the proteins, and the preparation of the enzyme for X-ray crystal structure analysis can result in changes in the active site.[1a,9] A number of crystal structures for DMSO reductase[2] and sulfite oxidase[3] show both six and seven coordination about the molybdenum.[10]

Analogue reaction systems can be used to verify experimental data on the structure and reaction mechanism of complex enzyme systems. An effective analogue reaction system should have the following properties: it should (1) react catalytically with enzyme substrates, (2) have similar kinetics, (3) have a similar structure, (4) not be complicated by the formation of a biologically irrelevant species, and (5) be well-characterized through X-ray crystallography.[10] In the past 20 years, a number of analogue reaction systems have been developed to model the properties of the molybdenum oxotransferase enzymes.[7,11−14]

In the analogue reaction system developed by Xiao et al.,[7] a bulky hydrotris(3,5-dimethyl-1pyrazolyl)borate ligand (MoO_2-(SPh)Tp) was shown to reduce DMSO and catalytically oxidize PPh_3 through a $Mo^VO(OH)$(SPh)Tp intermediate. This catalytic cycle, which mimics the physical and chemical processes known for the molybdenum oxotransferases, was studied theoretically by Pietsch and Hall[15] with a simplified model ($MoO_x(NH_3)_2$-$(SH)_2$, $x = 1$ or 2, with C_{2v} or C_2 symmetry imposed). Their results indicated that the primary oxygen atom transfer occurred through an associated intermediate and that the "spectator" oxygen played an important role in the reactivity of these compounds, as suggested by Rappé and Goddard.[16] Recently, an associative intermediate for a similar system (MoO(OPh)-$(OPEt_3)$(Tp′) (Tp′ = hydrotris(3-isopropylpyrazol-1-yl)borate))

Scheme 2

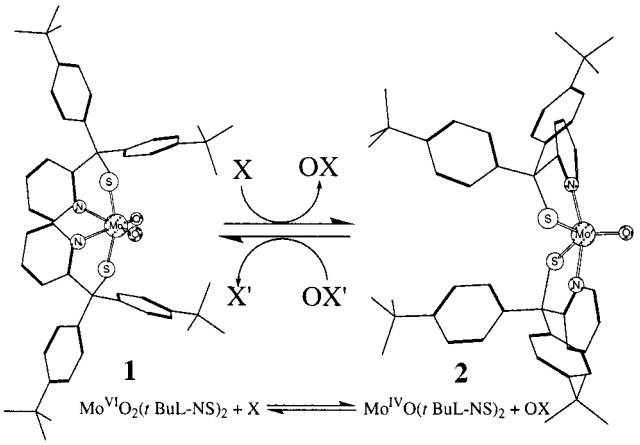

was characterized[17] through X-ray crystallography, which lends further support to the associative intermediate predicted by Pietsch and Hall.[15]

Deeth and co-workers[18] performed a theoretical investigation of an experimental model ($MoO_2(mnt)_2^{2-}$, mnt^{2-} = 1,2-dicyanoethylenedithiolate)[12] for sulfite oxidase. Two proposed mechanisms were studied for this system: a direct attack of hydrogen sulfite on the molybdenum center with formation of a seven-coordinate intermediate and a direct attack on one of the terminal oxo groups. Their results indicated that the lone pair on the sulfur atom attacked the terminal oxo group and proceeded to a six-coordinate intermediate through a barrier of 21.5 kcal/mol. The transition state for a direct attack on the molybdenum center was investigated, but was found to be more than 12 kcal/mol higher in energy than the first transition state in the oxo attack mechanism.

Inscore et al.[13] performed electronic absorption, magnetic circular dichroism (MCD), and resonance Raman spectroscopy on MoO(X)Tp (Tp = hydrotris(3,5-dimethyl-1-pyrazolyl)borate; X = 1,2-benzenedithiolate (bdt); 3,4-toluenedithiolate (tdt)) compounds and ab initio calculations on an ethenedithiolate fragment to ascertain the role of the MPT ligands in the molybdoenzymes. They found that there are two important low-energy LMCT (ligand-to-metal charge transfer) bands in these systems that involve the dithiolate ligand. One of the LMCT bands involves a three-center pseudo-σ-type bonding between the in-plane sulfur-based dithiolate p orbitals and the d_{xy} orbital of the molybdenum center. This three-center pseudo-σ interaction is thought to modulate the reduction potential of these systems by destabilizing the d_{xy} orbital. Their results also indicate that the "spectator" oxygen is important, because it controls the orientation of the occupied molybdenum d orbital thereby effecting the degree of bonding between the dithiolate ligand and the Mo.

An analogue reaction system developed by Schultz and Holm[11] is shown in Scheme 2. This system represents the most comprehensive study of the reverse oxo transfer reaction with an experimental model system to date. This analogue has been shown to undergo primary oxygen atom transfer through ^{18}O isotopic labeling studies and to react stoichiometrically with a wide range of substrates, including the enzyme substrates: Me_3-NO, arylamine *N*-oxides, Me_2SO, Ph_2SO, and IO_4^-. Each of the substrates studied exhibited well-behaved second-order

(9) Sjölin, L. *Crystallographically Determined Structures of Some Biologically Important Macromolecules*; Chapman & Hall: New York, 1996.

(10) Li, Hung-Kei; Temple C.; Rajagopalan, K. V.; Schindelin, H. *J. Am. Chem. Soc.* **2000**, *122*, 7673.

(11) (a) Schultz, B. E.; Gheller, S. F.; Muetterties, M. C.; Scott, M. J.; Holm, R. H. *J. Am. Chem. Soc.* **1993**, *115*, 2714. (b) Schultz, B. E.; Holm, R. H. *Inorg. Chem.* **1993**, *32*, 4244.

(12) (a) Das, S. K.; Chaudhury, P. K.; Biswas, D.; Sarkar, S. *J. Am. Chem. Soc.* **1994**, *116*, 9061. (b) Chaudhury, P. K.; Das, S. K.; Sarkar, S. *Biochem. J* **1996**, *319*, 953. (c) Lorber, C.; Plutino, M. R.; Elding, L. I.; Nordlander, E. *J. Chem. Soc., Dalton Trans.* **1997**, 3997.

(13) (a) Inscore, F. E.; McNaughton, R.; Westcott, B. L.; Helton, M. E.; Jones, R.; Dhawan, I. K.; Enemark, J. H.; Kirk, M. L. *Inorg. Chem.* **1999**, *38*, 1401. (b) Jones, R. M.; Inscore, F. E.; Hille, R.; Kirk, M. L. *Inorg. Chem.* **1999**, *38*, 4963.

(14) Oku, H.; Ueyama, N.; Nakamura, A. *Inorg. Chem.* **1997**, *36*, 1504.

(15) Pietsch, M. A.; Hall, M. B. *Inorg. Chem.* **1996**, *35*, 1273.

(16) Rappé, A. K.; Goddard, W. A., III *J. Am. Chem. Soc.* **1982**, *104*, 3287.

(17) Smith, P. D.; Millar, A. J.; Young, C. G.; Ghosh, A.; Basu, P *J. Am. Chem. Soc.* **2000**, *122*, 9298.

(18) Thrapper, A.; Deeth, R. J.; Nordlander, E. *Inorg. Chem.* **1999**, *38*, 1015.

Scheme 3

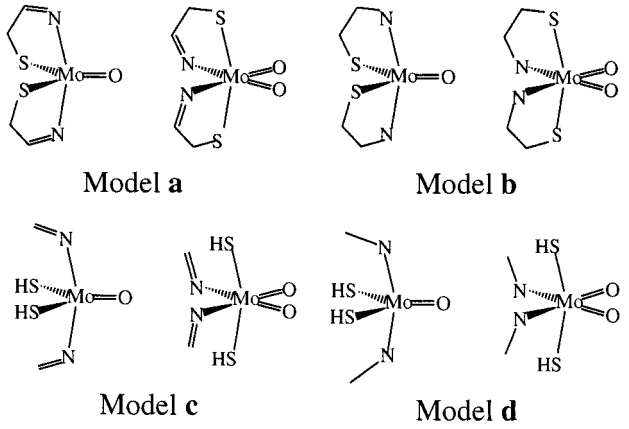

kinetics with large negative activation entropies. The large negative activation entropy indicates that there is an associative transition state in the rate-controlling step of the reaction mechanism. The bulky ligand (*t*-BuL-NS = bis(4-*tert*-butylphenyl)-2-pyridylmethanethiolate(1−)) used in this system inhibited the formation of the biologically irrelevant μ-oxo Mo(V) dimer under the reaction conditions used in their study. The system developed by Schultz and Holm is also interesting because of the significant ligand rearrangement upon reduction. In the six-coordinate $Mo(VI)O_2$ form the sulfur atoms are trans (*t*-S) but upon reduction to the five-coordinate Mo(IV)O, the molecule takes on a distorted trigonal bipyramidal structure and the nitrogens are now trans (*t*-N), shown in Scheme 2. This model system is most closely related to the oxotransferase systems that only contain terminal oxo groups (sulfite oxidase and DMSO reductase families).

In this study, the forces behind the ligand rearrangement (*t*-S in the dioxo to *t*-N in the monooxo) will be investigated, at the density functional level of theory, through four model systems (Scheme 3): **a** = $MoO_x(SCH_2CHNH)_2$, **b** = $MoO_x(SH)_2(CH_2NH)_2$, **c** = $MoO_x(SCH_2CH_2NH_2)_2$, and **d** = $MoO_x(SH)_2(NHCH_3)_2$ (x = 1 or 2). Compared to model **a**, models **b**, **c**, and **d** systematically remove the chelating character and unsaturation at the N, to investigate their effect on the energetics of the cis and trans isomers. Because model **a** gives the best representation of the experimental system, it will be used to investigate the reaction mechanism of **1a** + $P(CH_3)_3$ → **2a** + $OP(CH_3)_3$ at the density functional level. Even though model **a** gives a good representation of the electronic environment around the molybdenum center, it does not include the steric effects of the bulky 4-*tert*-butylphenyl groups, which we modeled by molecular mechanics. Our theoretical results for the reaction **1a** + $P(CH_3)_3$ → **2a** + $OP(CH_3)_3$ will be compared to the experimental results by Schultz and Holm for the reaction **1** + $P(CH_3CH_2)_3$ → **2** + $OP(CH_3CH_2)_3$. This study represents the first theoretical investigation of a molybdenum oxo transfer reaction, where all species in the reaction mechanism are fully optimized and characterized at the density functional level of theory.

Theoretical Details

All models were optimized in C_2 symmetry except the intermediate and transition states for model **a**, for which C_1 symmetry was employed. Models **a**, **b**, **c**, and **d** were optimized by using density functional theory (DFT),[19] with the Becke3 hybrid exchange functional and the Perdew86 correlation functional (B3P86).[20] Previous theoretical work has shown that the B3P86 functional gives similar, and sometimes superior, results to the B3LYP functional.[21] The substrate used in this study is $P(CH_3)_3$. The use of PH_3 as a ligand would decrease the computational cost, but it has been shown to give a poor representation for PR_3.[15] The exothermicity of the reaction $P(CH_3)_3 + {}^1/_2O_2 \rightarrow OP(CH_3)_3$ was experimentally determined to be 80(3) kcal/mol.[22] For this reaction, B3P86 calculations give an exothermicity of 61 kcal/mol, while B3LYP gives an exothermicity of 58 kcal/mol.[23] Therefore, B3P86 gives a slightly better representation of the O−P bond energy in $OP(CH_3)_3$, which is important to properly describe these molybdenum oxo transfer reactions with $P(CH_3)_3$. In a similar model system, Pietsch, Couty, and Hall have shown that Hartree−Fock (HF)[24] and Møller−Plesset second-order perturbation (MP2)[25] do not describe the molybdenum−oxygen bond properly, but variational correlation calculations and MP3 produce similar results.[26] Zaric and Hall have shown that DFT also produces reasonable results in this system.[27]

All calculations were performed with the Gaussian 94 (G94)[28] suite of programs using a full double-ζ basis set on the C, N, S, O, and H atoms and a double-ζ basis set plus one polarization function[29] on the P atom to properly describe the hypervalent character of phosphorus compounds. A small core ECP[30] was used for the Mo atom (1s2s2p3s3p3d) with a double-ζ quality basis set that includes the outer 5p function developed by Couty and Hall with a splitting of (541/541/31).[31]

Results and Discussion

Comparison of the Experimental Structure to the Optimized Geometry of the Model System. Due to the size of the experimental system, a smaller model must be used to represent it for the quantum chemical modeling. The two distinctive features of the immediate environment around the molybdenum center are the chelate ring constraint and aromatic N. In model **a**, the *t*-BuL-NS ligands were replaced with SCH_2CHNH ligands, which have similar sized chelate rings and are unsaturated at N.

The B3P86 C_2 optimized geometries for model **a**, **1a** and **2a**, can be found in Figure 1 along with the X-ray crystal structures, **1** and **2**. The optimized geometry of **1a** is a distorted octahedron with the sulfur and nitrogen atoms bent away from the oxo groups, and with the equatorial nitrogens twisted out

(19) Parr, R. G.; Yang, W. *Density-functional theory of atoms and molecules*; Oxford University Press: Oxford, 1989.

(20) (a) Becke, A. D. *Phys. Rev. A* **1988**, *38*, 3098. (b) Perdew, J. P. *Phys. Rev. B* **1992**, *45*, 13244.

(21) (a) Neumann, R.; Nobes, R. H.; Handy, N. C. *Mol. Phys.* **1996**, *87*, 1. (b) Wilberg, K. B.; Stratmann, R. E.; Frisch, M. J. *Chem. Phys. Lett.* **1998**, *297*, 60. (c) Arulmozhiraha, S.; Kolandaivel, P.; Ohashi, O. *J. Phys. Chem.* **1999**, *103*, 3073.

(22) Cox, J. D.; Pilcher, G. *Thermochemistry of Organic and Organometallic Compounds*; Academic Press: New York, 1970; pp 478−482.

(23) The B3P86 and B3LYP exothermicities include zero-point energies and thermal corrections.

(24) Roothaan, C. C. *J. Tev. Mod. Phys.* **1960**, *32*, 179.

(25) (a) Møller, C.; Plesset M. S. *Phys. Rev.* **1936**, *46*, 618. (b) Pople, J. A.; Binkley, J. S.; Seeger, R. *Int. J. Quantum Chem.* **1976**, *S10*, 1.

(26) Pietsch, M. A.; Couty, M.; Hall, M. B. *J. Phys. Chem.* **1995**, *99*, 16315.

(27) Zaric, S.; Hall, M. B. *Molecular Modeling and Dynamics of Bioinorganic Systems 3. High Technology*; Kluwer Academic Publishers: Dordrecht, 1997; Vol. 41, p 255.

(28) Frisch, M. J.; Trucks, G. W.; Schlegel, H. B.; Gill, P. M. W.; Johnson, B. G.; Robb, M. A.; Cheeseman, J. R.; Keith, T.; Petersson, G. A.; Montgomery, J. A.; Raghavachari, K.; Al-Laham, M. A.; Zakrzewski, V. G.; Ortiz, J. V.; Foresman, J. B.; Cioslowski, J.; Stefanov, B. B.; Nanayakkara, A.; Challacombe, M.; Peng, C. Y.; Ayala, P. Y.; Chen, W.; Wong, M. W.; Andres, J. L.; Replogle, E. S.; Gomperts, R.; Martin, R. L.; Fox, D. J.; Binkley, J. S.; Defrees, D. J.; Baker, J.; Stewart, J. P.; Head-Gordon, M.; Gonzalez, C. *Gaussian 94*, Revision D.4; Gaussian Inc., Pittsburgh, PA, 1995.

(29) Dunning, T. H., Jr.; Hay, P. J. *Modern Theoretical Chemistry*; Schaefer, H. F., III, Ed.; Plenum: New York, 1976; p 1.

(30) LaJohn, L. A.; Christiansen, P. S.; Ross, R. B.; Atashroo, T.; Ermler, W. C. *J. Chem. Phys.* **1987**, *87*, 2812.

(31) Couty, M.; Hall, M. B. *J. Comput. Chem.* **1996**, *17*, 1359.

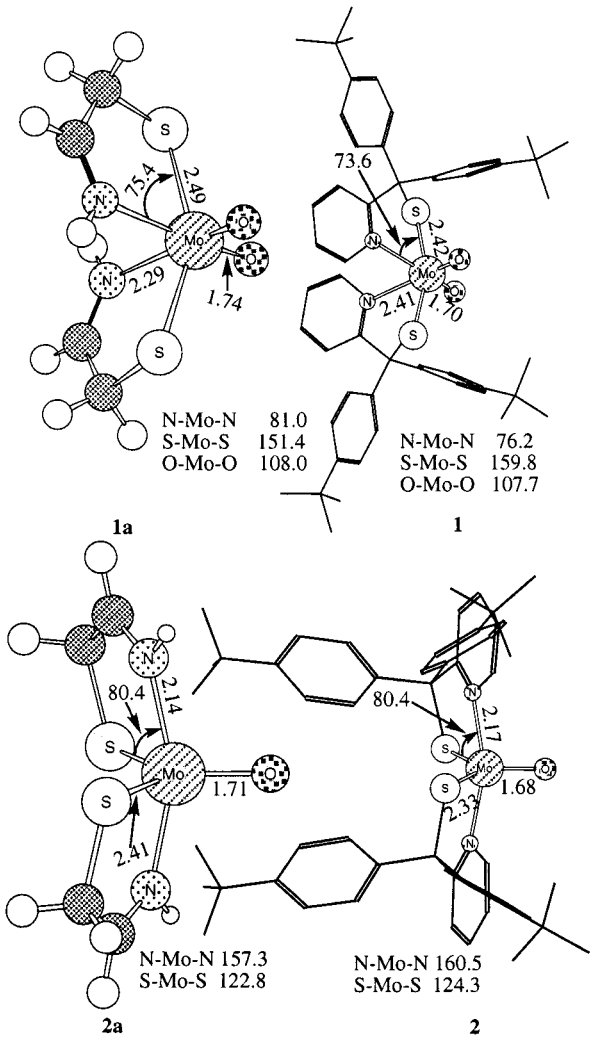

Figure 1. A comparison of the B3P86 C_2 optimized geometries for model **a**: *t*-S dioxo, **1a**, and *t*-N monooxo, **2a**, to the X-ray crystal structure data for the analogue system, **1** and **2**.

of the O−Mo−O plane by 11° ("twist" angle). The optimized geometry of **2a** is a distorted trigonal bipyramidal structure with the nitrogen atoms bent away from the oxo group. The bite angle (S−Mo−N) in **1a** is within 1.8° of that in **1**, and the bite angle in **2a** perfectly reproduces the experimental angle in **2**. The experimental N−Mo−N and S−Mo−S angles of **1** and **2** were reproduced to within 5° in **1a** and **2a** except for the S−Mo−S angle in **1a**, which is 8.4° smaller than that in **1**. The Mo−S bond distances are within 0.07−0.09 Å of the experimental system and the Mo−O bond distances are within 0.04 Å. However, the Mo−N bond distance in **1a** is 0.12 Å shorter than that in **1**. This difference was surprising since the Mo−N bond distance in **2** was reproduced to within 0.03 Å in **2a**.

To investigate why there was such a large discrepancy in the Mo−N bond distance in **1a** compared to that in the experimental system, the Hs on the nitrogen atoms were replaced with methyl groups. The optimized geometry showed an increase in the Mo−N bond distance to 2.38 Å (reducing the error from 0.12 to 0.03 Å) and the S−Mo−S angle opened up to 159.2° (reducing the error from 8.4° to 0.6°). However, adding the methyl group had very little effect on the rest of the structure and decreased the Mo−O bond distance by less than 0.01 Å. In **2**, the nitrogens are in the trans position, and there is very little steric hindrance due to the group attached to the nitrogens; therefore, **2a** reproduced the bond distance and angles in the

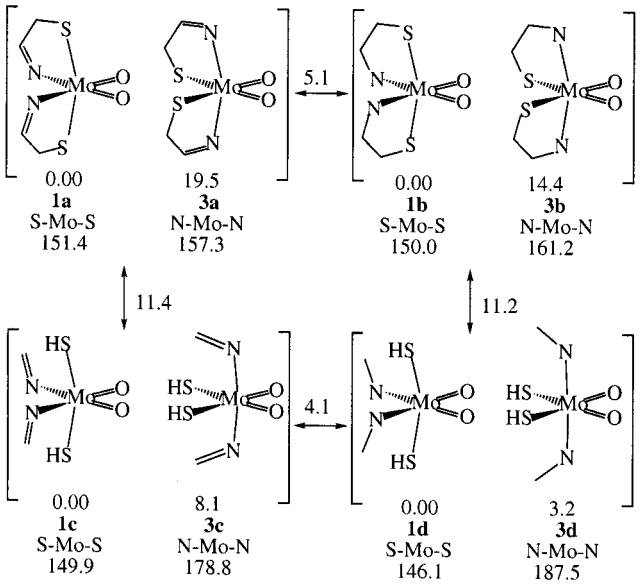

Figure 2. Relative energies (E(0K)) in kcal/mol for the B3P86 C_2 optimized dioxo isomers (*t*-S and *t*-N) for models **a**, **b**, **c**, and **d**. Energy values given above the arrows represent the change in energy difference of the two isomers between the respective models.

X-ray crystal structure. Since the addition of the methyl groups had very little effect on the geometry of the rest of **1a**, it was considered unnecessary to properly describe the oxygen atom transfer reaction, and would merely increase the computational cost with very little benefit.

Driving Force Behind the Ligand Rearrangement. There are two possible isomers for the dioxo (*t*-S dioxo (**1a**), *t*-N dioxo (**3a**)) and the monooxo species (*t*-N monooxo (**2a**), *t*-S monooxo (**4a**)). The energetics for both isomers were investigated for models **a**, **b**, **c**, and **d** (Scheme 3), in which the chelate character and unsaturation at the nitrogen were systematically removed. Model **b** retains the chelate character, but the ring is saturated, model **c** removes the chelate character while maintaining the unsaturation, and model **d** both removes the chelate character and saturates the ring. Models **c** and **d** used an SH ligand instead of an SCH_3 ligand because geometry optimizations with SCH_3 had convergence problems. These problems arose because the use of an SCH_3 ligand introduced unrealistic steric effects due to its close proximity with the H atoms of the $NHCH_2$ or NH_2-CH_3 in models **c** and **d**, respectively. This unrealistic steric effect would interfere with the investigation of the ring strain and electronic effects of the unsaturation on the energetics of the two isomers.

The *t*-S dioxo species is expected to be more stable than the *t*-N dioxo species because the strongest binding oxo groups want the weaker datively bound ligands trans to them, forcing the sulfur ligands into the trans position. In model **a**, the *t*-N dioxo isomer (**3a**) is 19.5 kcal/mol higher in energy than the *t*-S dioxo isomer (**1a**), as shown in Figure 2. When the ring is saturated (model **b**) the difference in energy between **1b** and **3b** drops to 14.4 kcal/mol. At this point, it was unclear as to whether the drop in energy was due to the saturation of the nitrogen or a release in some of the ring strain. When the chelating ring is clipped open but the unsaturation is retained (model **c**) the difference in energy between **1c** and **3c** is 8.1 kcal/mol. Figure 2 shows that the S−Mo−S angle does not change significantly from **1a** to **1c** (151.4° to 149.9°, respectively), but the N−Mo−N angle changes from 157.3° (**3a**) to 178.8° (**3c**), in the *t*-N isomers. These results indicate that when the sulfur ligands are trans to each other they prefer to be bent away from

the oxygen ligands, but when the nitrogen ligands are trans, they prefer to be approximately 180.0° from each other. Therefore, the chelating ring in the *t*-N isomer forces the N−Mo−N angle to decrease from its preferred 180°, and consequently increases the energy. In the *t*-S isomer, the S−Mo−S angle in the chelate ring is within 4° of the natural (unchelated) angle; therefore, the chelate ring has very little effect on the *t*-S isomer's energy. Removing the chelating ring and saturating the nitrogen (model **d**) decreased the difference in energy between **1d** and **3d** to only 3.2 kcal/mol.

Overall, the trans influence alone was found to account for 3.2 kcal/mol difference in energy between the *t*-S and *t*-N dioxo species. Inclusion of the ring strain increases the difference in energy by another 11 kcal/mol and the unsaturated nitrogens increase the difference in energy of the isomers by another 4−5 kcal/mol. Therefore, the trans influence accounts for approximately 16% of the energy difference, the unsaturated nitrogen accounts for 26% of the energy difference, and the ring strain accounts for 58% of the energy difference between the two isomers.

The sulfur ligands prefer not to be trans to each other because they have stronger (more covalent) bonds to Mo than the nitrogen groups. Since the monooxo species is a distorted trigonal bipyramidal structure, no ligand is trans to the strongest binding oxo ligand and the sulfurs no longer have to be trans to each other as in the dioxo species. For all of the model systems studied, the *t*-S monooxo species (**4a**, **4b**, **4c**, and **4d**) is not a stable geometry. Geometry optimizations begun with a *t*-S structure always reverted to the *t*-N geometry. Fixing the S−Mo−S angle to 159.8° (as found in the *t*-s X-ray crystal structure) resulted in species that were 8−11 kcal/mol higher in energy than the *t*-N monooxo species. The transformation of the monooxo species from a *t*-S to a *t*-N arrangement is a barrierless process via a Berry pseudorotation,[32] because there is no interference from the occupied Mo d orbital. Rearrangement in the dioxo species would require a Bailar or trigonal twist motion or one of a variety of ring-opening mechanisms.[32] Any of these rearrangement mechanisms would have to go over a barrier and that is why both *t*-N and *t*-S isomers are stable minima for the dioxo species.

Reaction Mechanism for the Primary Oxygen Atom Transfer. The experimental exothermicity of (*t*-BuL-NS)$_2$MoO + $^1/_2$O$_2$ → (*t*-BuL-NS)$_2$MoO$_2$ was estimated to be 43−79 kcal/mol.[11b] Model **a** has a calculated exothermicity ($\Delta H°$) of 42 kcal/mol for the reaction **2a** + $^1/_2$O$_2$ → **1a**, which is only 1 kcal/mol lower than the smallest value in the experimental range. An underestimation of the exothermicity of this reaction is not entirely surprising since the exothermicity ($\Delta H°$) of P(CH$_3$)$_3$ + $^1/_2$O$_2$ → OP(CH$_3$)$_3$ was underestimated by approximately 16 kcal/mol at this level of theory. Thus, model **a** appears to give a good structural and a reasonable energetic representation of the experimental system.

In the study of this reaction mechanism, it was important to optimize the reacting MoO$_2$ species with the explicit inclusion of the substrate, P(CH$_3$)$_3$, and to optimize the final MoO species with the explicit inclusion of the product, OP(CH$_3$)$_3$. This procedure reduces the problem of basis set superposition error (BSSE). The structures of **REAC** (MoO$_2$L$_2$···P(CH$_3$)$_3$) and **PROD** (MoOL$_2$···OP(CH$_3$)$_3$) are shown in Figure 3. The addition of the substrate to **1a** had very little effect on the structure of the MoO$_2$ structural parameters, Table 1. Bond distances in **REAC** were within 0.01 Å of **1a**, the N−Mo−N angle increased by 0.2°, the S−Mo−S angle increased by 0.6°, and the bite angle S−Mo−N increased by less than 0.1° in **REAC** compared to **1a**.

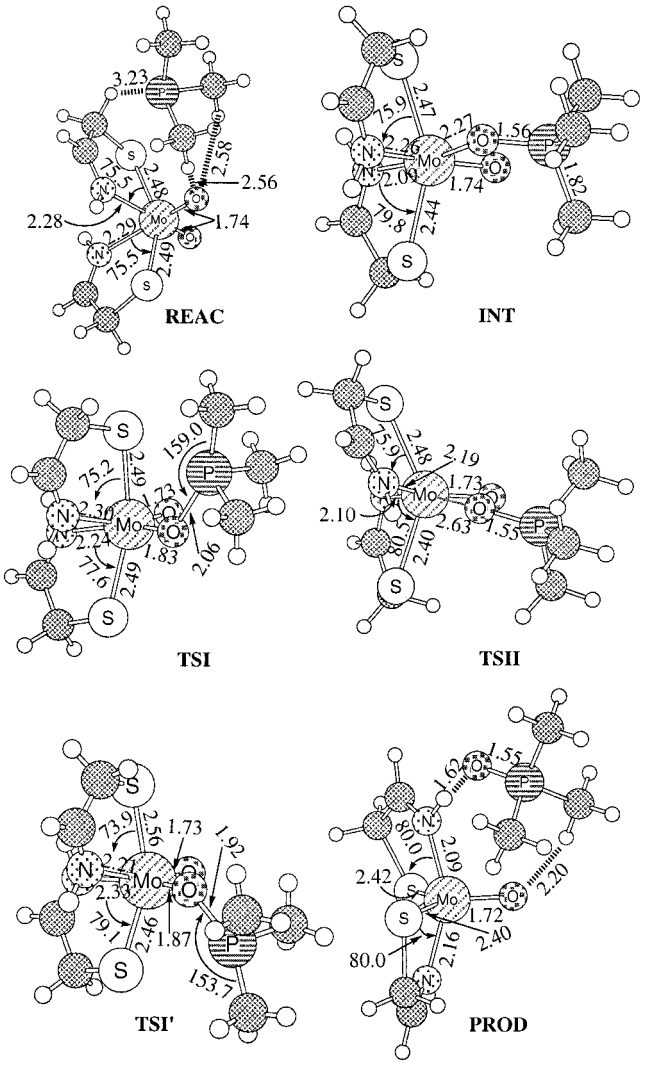

Figure 3. B3P86 optimized geometries for the reactant, **REAC**, first transition state, **TSI** and **TSI′**, intermediate, **INT**, second transition state, **TSII**, and the product, **PROD**. Important bond and dihedral angles can be found in Table 2.

Table 1. Important Bond Distances (Å) and Angles (deg) for **1a**, **REAC**, **1**, **2a**, **PROD**, and **2**

	1a	REAC	1	2a	PROD	2
Mo−O	1.74	1.74	1.70	1.71	1.72	1.68
Mo−S	2.49	2.48	2.42	2.41	2.40	2.33
Mo−S′	2.49	2.49	2.42	2.41	2.42	2.33
Mo−N	2.29	2.28	2.41	2.14	2.09	2.17
Mo−N′	2.29	2.29	2.41	2.14	2.16	2.17
S−Mo−N	75.4	75.5	73.6	80.4	80.0	80.4
S−Mo−S	151.4	152.0	159.8	122.8	129.4	124.3
N−Mo−N	81.0	81.2	76.2	157.3	150.0	160.5
O−Mo−O	108.0	108.0	107.7			
N−O−Mo−O	169.0	169.0	167.7			
"twist"	11.0	11.0	12.6			

As mentioned in the Introduction, the second terminal oxo group in the reacting species is called a spectator ligand because it does not participate in the reaction directly, but it is more important for this reaction than other spectator ligands. MoO$_2$ can only have a maximum bond order of 5; therefore, each MoO bond has an order of 2.5, but in MoO the Mo−O can have a

(32) Cotton, F. A.; Wilkinson, G. *Advanced Inorganic Chemistry: A Comprehensive Text*, 4th ed.; Wiley-Interscience Publication: New York, 1980; pp 1218−1226.

Table 2. Important Bond and Dihedral Angles (deg) for the **REAC**, **TSI**, **TSI′**, **Int**, **TSII**, and **PROD**, Shown in Figure 3

	S−Mo−S	N−Mo−N	O−Mo−O	P−O−Mo	P−O−Mo−O
REAC	152.0	81.2	108.0		
TSI	158.3	80.7	105.7	125.7	77.6
TSI′	153.8	79.5	105.3	135.0	−71.8
INT	150.3	97.6	84.4	123.3	−6.9
TSII	138.8	123.5	75.6	119.7	−13.8
PROD	129.4	150.0			

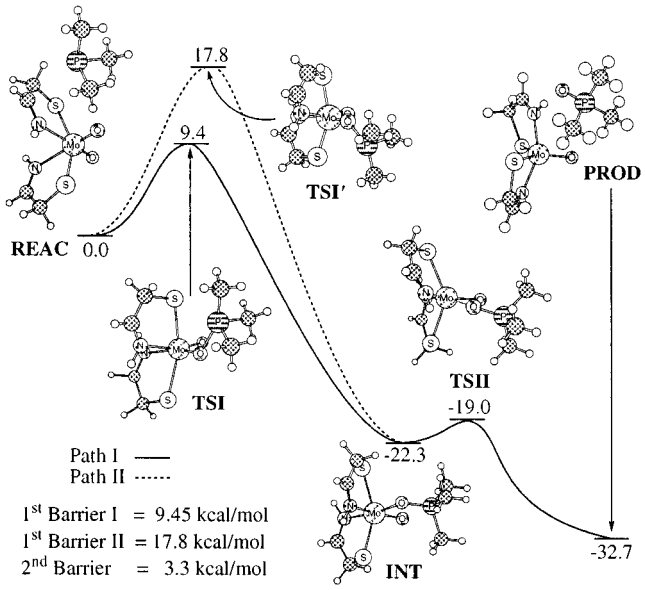

Figure 4. The reaction path for **1a** + $P(CH_3)_3$ → **2a** + $OP(CH_3)_3$, where **REAC** is **1a** optimized with the explicit inclusion of the substrate $P(CH_3)_3$, **TSI** is the first transition state, **TSI′** is the first transition state of a higher energy reaction path, **INT** is the intermediate, **TSII** is the second transition state, and **PROD** is **2a** optimized with the explicit inclusion of the product $OP(CH_3)_3$. Energies are in kcal/mol and include zero-point energy (ZPE) and thermal corrections.

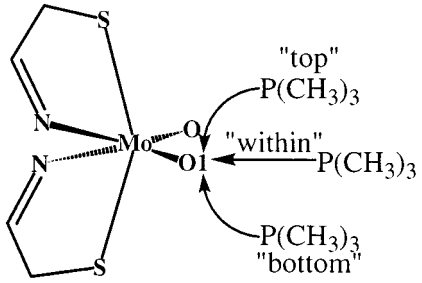

Figure 5. Three possible approaches for the attack of the substrate $P(CH_3)_3$ on **1a**: "top", "within", and "bottom".

bond order of 3.[33] The spectator oxygen makes the active oxygen more susceptible to attack by keeping it from forming a formal triple bond with the molybdenum and then strengthens its own bond as substrate attack weakens the other Mo−O bond.

The mechanism for the reaction of **1a** with $P(CH_3)_3$, (**REAC** → **PROD**), determined at the B3P86 level of theory, is shown in Figure 4. Several approaches for substrate attack on one of the terminal oxo groups were investigated. Three of the possible approaches are shown in Figure 5, and are labeled "top", "within", and "bottom". The labels are in reference to the location of substrate attack on the terminal oxo group labeled O1 (Figure 5) relative to the O−Mo−O plane. An approach from "within" the O−Mo−O plane was found not to be a transition state, but the "top" and "bottom" approaches did produce 1st order saddle points, **TSI** and **TSI′**, respectively. At first glance, it was suspected that the "bottom" approach would be energetically more favorable than the "top" approach due to the sterics of the chelate ring, but it was found that the "top" approach was 8.4 kcal/mol lower in energy. A picture of the 0.05 contour surface of the highest occupied molecular orbital (HOMO) of **2a** (Figure 6a) helps to explain why the "top" approach is energetically more favorable for this model. The significant "twist" (11.0°) about the equatorial region of **1a** causes the lone pair orbitals on the oxygen ligands to rotate. The lone pair lobe pointing "up" is more accessible than the lower lobe; therefore, the "top" approach is electronically favored.

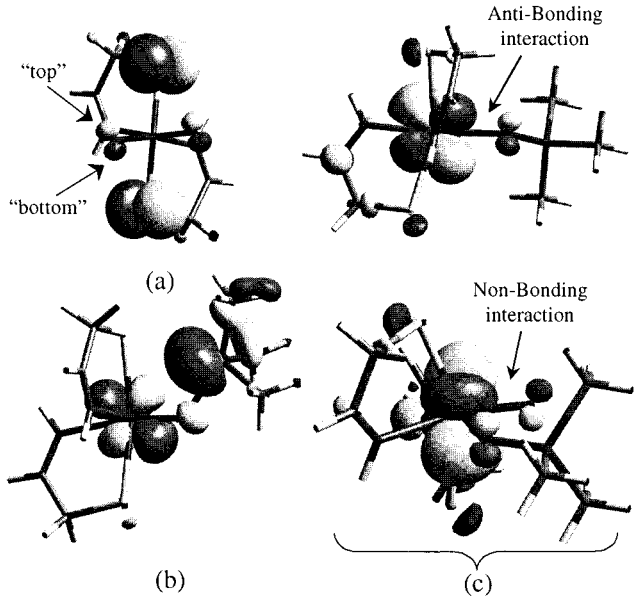

Figure 6. Picture of the 0.05 contour surface diagram of the highest occupied molecular orbital (HOMO) of (a) **1a**, (b) **TSI**, and (c) **INT**.

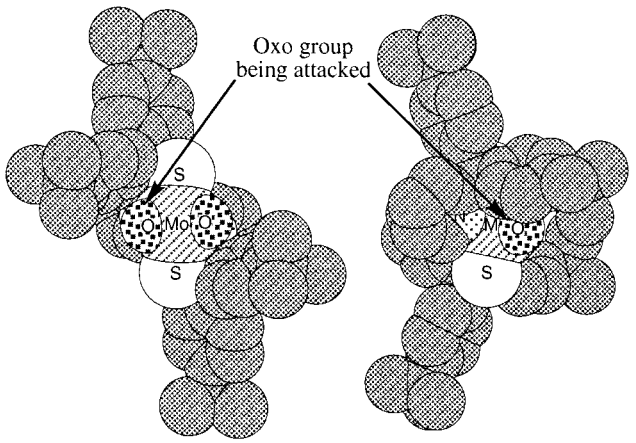

Figure 7. Space-filled model representation of the experimental model, **1**, from two perspectives. The hydrogen atoms were excluded for clarity.

A comparison of **1a** with **1** shows that the "top" approach might have significant steric repulsion due to the substituted phenyl ring that lies over the terminal oxo being attacked. Figure 7 shows a space-filled model of the analogue system, **1**, from two perspectives and clearly shows that the "top" approach would be sterically hindered. To gain an estimate of how flexible

(33) Lin, Z. Y.; Hall, M. B. *Coord. Chem. Rev.* **1994**, *123*, 149.

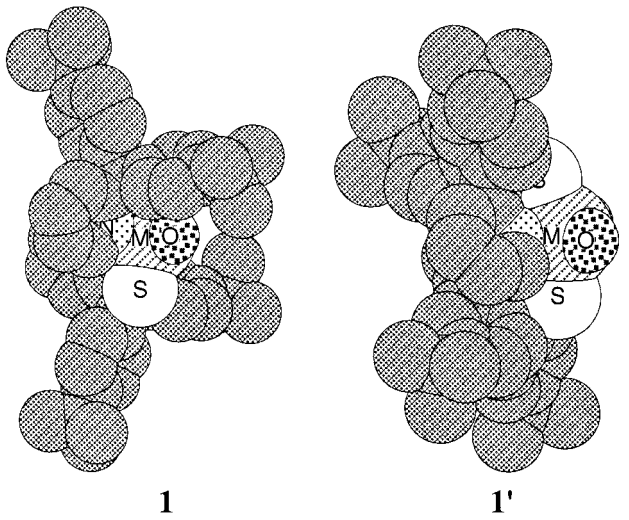

Figure 8. Two possible conformations, **1** and **1′**, found from the UFF optimized structure of **1**, with the atoms attached to the Mo frozen at the B3P86 optimized values of **1a**. The hydrogen atoms were not included for clarity.

the bulky ligands would be, a few simple molecular mechanic calculations were performed using the open force field (OFF) module in the Cerius[2] suite of programs.[34] The *t*-BuL ligand was added to the B3P86 optimized **1a,** and the atoms attached to the Mo were frozen, while the rest of the structure was optimized with use of the universal force field (UFF).[35] It was found that there were two stable conformations, **1** and **1′**, for this model, shown in Figure 8. The conformation shown as **1** in Figure 8 is similar to the crystal structure where the substituted phenyl ring is lying over the "top" of the oxo ligand but the other conformation, **1′**, leaves the oxo ligand free of the substituted phenyl ring. At the UFF level of theory, **1′** was found to be 5.2 kcal/mol higher in energy than **1**. Since the core atoms in both isomers (**1** and **1′**) were frozen at the optimized values in **1a**, it is likely that the difference in their energy is even smaller.[36] It is possible that in solution both conformations, **1** and **1′**, are available for reaction with the substrate, $P(CH_3)_3$. Therefore, "top" attack on **1′** may have no more steric hindrance than "bottom" attack.

In the lowest energy first transition state, **TSI**, the $P(CH_3)_3$ attacks the reactive oxo group from the "top", pushing the electron pair involved in the Mo−O π bond into the Mo d_{xy} orbital, shown in Figure 6b. The bonding between the reactive oxygen and the attacking substrate appears to be unusual. The ideal angle for C−P−O in the product would be approximately 109.5°, but the C−P−O angle found in **TSI** is 159.0° and the other two C−P−O angles are close to 90° (Figure 3). These angles suggest that in the transition state the C−P−O engages in a 3-center, 4-electron interaction (3c-4e$^-$). To determine if this was a steric effect, the C−P−O angles were changed to 109.5° without changing the rest of the structure. The closest contact of the H atoms on the $P(CH_3)_3$ group to any other atom was 1.9 Å. This lack of steric interference suggests that the C−P−O angle of 159.0° in **TSI** is due to an electronic effect. **TSI′** also exhibited a large C−P−O angle (153.7°).

(34) Cerius[2] version 4.2 Molecular Simulations Inc. (MSI), 1999.

(35) (a) Rappé, A. K.; Colwell, K. S.; Casewit, C. J. *Inorg. Chem.* **1993**, *32*, 3438. (b) Rappé, A. K.; Casewit, C. J.; Colwell, K. S.; Goddard, W. A., III; Skiff, W. M. *J. Am. Chem. Soc.* **1992**, *114*, 10024. (c) Casewit, C. J.; Colwell, K. S.; Rappé, A. K. *J. Am. Chem. Soc.* **1992**, *114*, 10035.

(36) (a) Beachy, M. D.; Chasman, D.; Murphy, R. B.; Halgren, T. A.; Friesner, R. A. *J. Am. Chem. Soc.* **1997**, *119*, 5908. (b) Gundertofte, K.; Liljefors, T.; Norrby, Per-Ola; Pettersson, I. *J. Comput. Chem.* **1996**, *17*, 429.

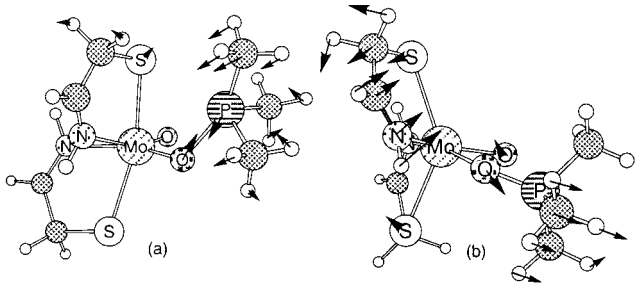

Figure 9. Vector representation of the normal coordinate for the imaginary frequency of (a) **TSI** and (b) **TSII**.

A frequency calculation was performed on the transition state, **TSI**, and one imaginary frequency was found (175.9*i* cm^{-1}) whose normal coordinate corresponds to the formation of the P−O bond and the weakening of the Mo−O bond with very little movement of the chelate ligands (Figure 9a). A frequency calculation of **TSI′** was also performed and one imaginary frequency was found (316.1*i* cm^{-1}) whose normal coordinate also corresponds to the formation of the P−O bond and the weakening of the Mo−O bond.

The first transition state, **TSI**, barrier is 9.4 kcal/mol, which is within the experimental uncertainty for the $\Delta H^{\ddagger}$ of the reaction **1** + $P(C_2H_5)_3$ → **2** + $OP(C_2H_5)_3$ ($\Delta H^{\ddagger}$ = 9.6(6) kcal/mol).[11] The inclusion of the bulky ligands would probably increase the calculated transition state barrier. The associative transition state, **TSI**, has a calculated $\Delta S^{\ddagger}$ of −16 eu, which is in qualitative agreement with the experimentally determined entropy of activation ($\Delta S^{\ddagger}$ = −37(2) eu).[11]

From the first transition state to the intermediate, **INT**, the $OP(CH_3)_3$ group rotates to lie almost in the O−Mo−O plane of the intermediate, O−Mo−O−P dihedral −6.9° (Figure 3), and loses the unusual 3c-4e$^-$ interaction (O−P−C) found in **TSI**. This motion weakens the Mo−O bond because it causes the remaining oxygen p_π lone pair to interfere destructively with the now occupied d_{xy} (Figure 6c). The occupied d_{xy} orbital has very little effect on the Mo−O bond of the spectator oxygen since it is δ to the spectator O p_π lone pair orbital (Figure 6c). From **REAC** to **INT** there is very little change in the S−Mo−S angles (152.0° to 150.3°) and there is a small increase in the N−Mo−N angles (81.2° to 97.6°), so a significant amount of movement in the chelate ligands must occur later to achieve the *t*-N arrangement in the product, **PROD**. The exothermicity ($\Delta H°$) of the reaction to the intermediate (**REAC** → **INT**) is 22.3 kcal/mol.

Other geometric structures for the intermediate were investigated, and it was found that there was another structure close in energy to **INT**, but it had the harder N ligands in the trans orientation. For this intermediate to be on the reaction path, **1a** would first have to go through a barrier to its *t*-N isomer, and since the *t*-N isomer is 19.5 kcal/mol (ΔE) higher in energy, the *t*-N intermediate would lie on a significantly higher energy reaction path. Unlike the O−Mo−O−P dihedral angle of −6.9° in the *t*-S intermediate, **INT**, the O−Mo−O−P dihedral angle for the alternate *t*-N structure (*t*-N) is −68.0°. It appears that having the harder ligands in the trans position has a significant effect on the O−Mo−O−P dihedral angle of the intermediate. Recently, a crystal structure[17] was determined for the intermediate, $MoO(OPh)(Tp')(OPEt_3)$, from the reaction $MoO_2(OPh)(Tp') + PEt_3 \rightarrow MoO(OPh)(Tp') + OPEt_3$ (Tp′ = hydrotris(3-isopropylpyrazol-1-yl)borate) and the O−Mo−O−P dihedral angle was reported to be −57.5(3)°.

The reaction from **INT** to the second transition state, **TSII**, involves the weakening of the Mo−$OP(CH_3)_3$ bond and the

concomitant rearrangement of the ligands from the *t*-S to halfway between the *t*-S and the *t*-N arrangement with a barrier (**INT** → **TSII**) of 3.3 kcal/mol. A frequency calculation on **TSII** showed one imaginary frequency (76.0*i* cm^{-1}) whose normal coordinate corresponds to the $OP(CH_3)_3$ group leaving, the S−Mo−S angle decreasing, and the N−Mo−N angle increasing (Figure 9b). This result is consistent with the decrease in the S−Mo−S angle (150.3°to 138.8°) and the significant increase in the N−Mo−N angle (97.6° to 123.5°) from **INT** to **TSII**. The small second barrier (3.3 kcal/mol) would make it very difficult to capture the intermediate in this reaction for characterization, because the exothermicity of the first step is 22.3 kcal/mol, which provides more than enough energy to immediately send the intermediate to the products even if a large amount of the excess energy was dissipated to the solution. It may be possible to capture the intermediate for characterization by adding an excess of $OP(CH_3)_3$ to the product, **2**, thus shifting the equilibrium back to the intermediate.

Originally, for the reaction MoO + OX → MoO_2 + X it was hypothesized that either there was a rearrangement of the ligands before the substrate, OX, attacked the monooxo species or the rearrangement occurred with attack of the substrate.[11] Here, we have shown that the *t*-S MoO species is not a stable structure and by microscopic reversibility, the attack of Me_3PO must occur concomitantly with the ligand rearrangement.

Finally, with the loss of the product, $OP(CH_3)_3$, the N−Mo−N angle continues to increase from **TSII** → **PROD** (123.5° to 150.0°) and the S−Mo−S angle continues to decrease (138.8° → 129.4°) to afford the distorted trigonal bipyramidal *t*-N monooxo species, **PROD**. Without the explicit inclusion of the product, $OP(CH_3)_3$, it was found that the products energy (**1a** + $OP(CH_3)_3$) was higher than the energy in the second transition state, **TSII**. Therefore, it appears that solvation has an important effect on the energetics of this system. The overall exothermicity of **REAC** → **PROD** is 32.7 kcal/mol ($-\Delta H°$) and $\Delta G° = -27.1$ kcal/mol, a value consistent with the equilibrium lying far to the right.[37]

(37) PCM single-point energies were calculated for REAC, TSI, INT, TSII, and PROD. The PCM energetics were within 2 kcal/mol of the gas-phase energetics.

Conclusions

Density functional calculations showed that for the dioxo species there are two stable isomers, *t*-N and *t*-S, for all models studied, and that the *t*-N isomer was higher in energy than the *t*-S isomer. An analysis of the energetics for the two isomers, in four model systems, indicated that a trans influence accounted for approximately 16% of the energy difference, the unsaturation at the nitrogens accounted for ≈26%, and the ring strain from the chelator accounted for ≈58% of the energy difference between the two isomers (*t*-N and *t*-S). Calculations on the monooxo species showed that the *t*-S isomer was not a stable geometry for any of the models studied at the B3P86 level of theory due to a barrierless Berry pseudorotation to the stable *t*-N isomer.

Density functional calculations on $MoO_2(SCH_2CHNH)_2$ + $P(CH_3)_3$ → $MoO(SCH_2CHNH)_2$ + $OP(CH_3)_3$ indicate that this reaction proceeds through a two-step mechanism via an associative intermediate. The substrate was found to attack one of the terminal oxo groups from the "top" to form an unusual 3c-4e$^-$ O−P−C bond in the first transition state, **TSI**. The $OP(CH_3)_3$ group then rotates to almost lie in the MoO_2 plane to form the intermediate, **INT**. The second transition state, **TSII**, involves the weakening of the Mo−$OP(CH_3)_3$ bond and the concomitant rearrangement of the ligands. These results indicate that for the reverse oxo transfer reaction there would have to be a concomitant, instead of prior, rearrangement of the ligands with attack of an OX substrate, which is supported by the result that the *t*-S monooxo species is not a stable structure. The overall exothermicity of this reaction is 32.7 kcal/mol ($-\Delta H°$) and $\Delta G° = -27.1$ kcal/mol, a value consistent with the equilibrium lying far to the right. The $\Delta H^{\ddagger}$ for the first step (rate-determining) was found to be 9.4 kcal/mol, and the second step had a $\Delta H^{\ddagger} = 3.3$ kcal/mol. These results are within the uncertainty of the experimental system, for which the rate-determining $\Delta H^{\ddagger}$ was 9.6(6) kcal/mol.

Acknowledgment. We thank The Welch Foundation (A-648) and the National Science Foundation (CHE-9800184) for their generous support. We would also like to thank the Supercomputing Facility at Texas A&M University for computer time.

JA003258Y